

Direct Electron Transfer Enables Highly Efficient Dual Emission Modes of Mn²⁺-Doped Cs₂Na_{1-x}Ag_xBiCl₆ Double Perovskites

Min Wang, Jing Lyu, Xian Qin, Shuo-Wang Yang, Xiaogang Liu,* and Guo Qin Xu*

Cite This: *J. Phys. Chem. Lett.* 2022, 13, 9429–9434

Read Online

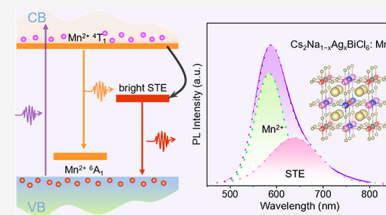
ACCESS |

Metrics & More

Article Recommendations

Supporting Information

ABSTRACT: Double perovskites with bright emission, low toxicity, and excellent stability have drawn considerable attention. Herein, we report the hydrothermal synthesis of Mn²⁺-doped Cs₂Na_{1-x}Ag_xBiCl₆ double perovskites that exhibit dual emission modes. Introducing Ag⁺ ions to Cs₂NaBiCl₆ samples enables a bright self-trapped exciton (STE) emission in orange-red color, whereas Mn²⁺ dopants induce a yellow-orange emission. Importantly, Mn²⁺ doping into Cs₂Na_{1-x}Ag_xBiCl₆ double perovskites with an indirect bandgap enables a high photoluminescence quantum yield of 49.52 ± 2%. Density functional theory calculations reveal that bringing Ag⁺ ions into Cs₂NaBiCl₆ can localize wave function to the [AgCl₆]⁵⁻ octahedron and convert dark transitions to bright STE transitions. Moreover, the 3d orbitals of Mn²⁺ dopants hybridize with Bi-6p and Cl-3p orbitals at the conduction band minimum, resulting in direct electron transfer from the host to Mn²⁺ and a significant increase in photoluminescence efficiency. These results shed light on the optical physical process of Mn²⁺-doped systems, providing useful information for further improvement of the photoluminescence efficiency of double perovskites.



Lead halide perovskites APbX₃ (A = CH₃NH₃⁺, CH₃(NH₂)₂⁺, Cs⁺; X = Cl⁻, Br⁻, I⁻) have attracted considerable attention in optoelectronic applications as excellent solution-processable semiconductors.^{1–3} However, the toxicity of lead and the environmental instability of lead halide perovskites have limited their practical applications.^{4,5} To address these problems, one strategy is to substitute Pb²⁺ with other ions from the IV group, such as Sn²⁺/Ge²⁺.⁶ However, Sn²⁺ and Ge²⁺ ions are easily oxidized to their tetravalent state (Sn⁴⁺/Ge⁴⁺) in air, resulting in poor structural stability. Another promising way is to replace two divalent Pb²⁺ with a monovalent cation and a trivalent cation, forming a quaternary lead-free halide double perovskite with the basic formula A₂M¹M²X₆ (A = Cs⁺; M¹ = Ag⁺, Na⁺; M² = Bi³⁺, In³⁺, Sb³⁺; X = Cl⁻, Br⁻, I⁻).⁷ Because of their low toxicity, high stability, and small carrier effective mass, double perovskites have been proposed as promising candidates for photoelectric detectors, LEDs, and photovoltaic applications.⁸ Compared with traditional lead halide perovskites, Cs₂AgBiBr₆ exhibits a long photoluminescence lifetime of ca. 660 ns and high photoexcited carrier density of 2.2 × 10¹⁶ cm⁻³.⁹

Despite their popularity in recent years, double perovskites have attracted great attention in recent years; they have weak PL and low power conversion efficiency due to their indirect bandgap or parity-forbidden direct bandgap.^{10–12} To date, alloying and doping serve as effective approaches to manipulate the bandgap of semiconductors. For example, a very high photoluminescence quantum yield (PLQY) of 86 ± 5% has been achieved in an alloyed Cs₂Ag_{1-x}Na_xInCl₆ system with Bi doping, which is several orders higher than that of pure Cs₂AgInCl₆ (PLQY < 0.1%).¹³ Of all the doped metals, Mn²⁺ is most frequently used to modulate the electronic structures

and optical properties of double perovskites, allowing the introduction of an additional emission channel originating from the ⁴T₁–⁶A₁ transition of the octahedral Mn²⁺.^{14–16} In Mn²⁺-doped double perovskite systems, most of the energy transfer processes usually take place from the STE state of the double perovskite to Mn²⁺ rather than directly from free electrons to Mn²⁺,^{14,17,18} which would generate a pronounced energy loss caused by the inevitable defects between the host and doped states.^{19,20} Therefore, realizing the direct energy transfer between the host and dopant is crucial for enhancing the PL efficiency of double perovskites.

In this work, we synthesized Mn²⁺-doped lead-free double perovskites Cs₂Na_{1-x}Ag_xBiCl₆ (0 ≤ x < 1) by the hydrothermal method. By optimizing the Na⁺/Ag⁺ ratio, the Cs₂Na_{0.98}Ag_{0.02}BiCl₆ sample exhibits a bright orange-red emission mode originating from the recombination of the bright STE state. Then, an additional yellow-orange emission mode of characteristic emission of Mn²⁺ is achieved when an appropriate amount of Mn²⁺ is doped into Cs₂Na_{0.98}Ag_{0.02}BiCl₆, with a highest PLQY of 49.52 ± 2%. The calculation results suggest that the introduced Ag⁺ is the key factor for the formation of the bright STE state and that the hybridizations of Mn-3d with Bi-6p and Cl-3p orbitals at the CBM in the doped systems give rise to direct electron

Received: August 31, 2022

Accepted: October 3, 2022

Published: October 4, 2022



transfer from the $\text{Cs}_2\text{Na}_{0.98}\text{Ag}_{0.02}\text{BiCl}_6$ host to Mn^{2+} dopants, resulting in highly efficient dual emission modes.

A hydrothermal method was employed to synthesize the Mn^{2+} -doped $\text{Cs}_2\text{Na}_{1-x}\text{Ag}_x\text{BiCl}_6$ ($0 \leq x < 1$) double perovskite (Supporting Information). Pure $\text{Cs}_2\text{NaBiCl}_6$ crystal adopts a space group $Fm\bar{3}m$, with alternating corner-sharing $[\text{NaCl}_6]^{5-}$ and $[\text{BiCl}_6]^{3-}$ octahedra and the Cs^+ cations in the framework cavities to maintain charge neutrality.^{21,22} Figure 1a shows the crystal structure of alloyed $\text{Cs}_2\text{Na}_{1-x}\text{Ag}_x\text{BiCl}_6$ in which the central $[\text{NaCl}_6]^{5-}$ octahedron is replaced by an $[\text{AgCl}_6]^{5-}$ octahedron. Powder X-ray diffraction (XRD) patterns of the

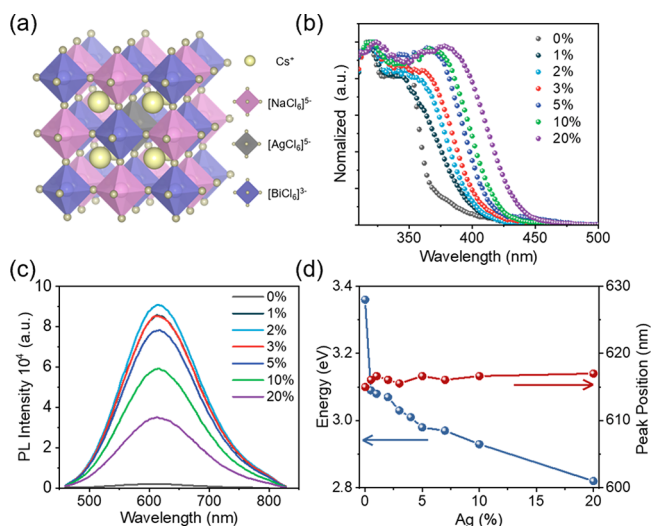


Figure 1. (a) Crystal structure of $\text{Cs}_2\text{Na}_{1-x}\text{Ag}_x\text{BiCl}_6$. (b) UV-vis absorption spectra and (c) PL spectra of alloyed $\text{Cs}_2\text{Na}_{1-x}\text{Ag}_x\text{BiCl}_6$ samples with different Ag^+ feeding ratios ($x = 0, 1, 2, 3, 5, 10,$ and 20%). (d) Bandgap and PL peak position of alloyed $\text{Cs}_2\text{Na}_{1-x}\text{Ag}_x\text{BiCl}_6$ samples as a function of Ag^+ feeding ratio.

as-prepared $\text{Cs}_2\text{Na}_{1-x}\text{Ag}_x\text{BiCl}_6$ samples with varying Ag^+/Na^+ ratios (0, 0.5, 1, 2, and 4%) are shown in Figure S1a. The alloyed samples can be well indexed into cubic $Fm\bar{3}m$ with no detectable impurities, indicating that Ag^+ ions do not change the crystal structure of the pure sample. In the enlarged view, the characteristic diffraction peak (i.e., at 14.76°) of the alloyed sample shifts to high angles with increasing Ag^+ content (Figure S1b) due to the lattice contraction caused by the replacement of Na^+ by the smaller Ag^+ .^{13,17}

X-ray photoelectron spectroscopy (XPS) (Figure S2) of the $\text{Cs}_2\text{Na}_{0.98}\text{Ag}_{0.02}\text{BiCl}_6$ sample shows that all elements are present in the expected oxidation state. Scanning electron microscopy–energy dispersive spectroscopy (SEM-EDS) mapping reveals that Ag^+ ions are uniformly distributed in the alloyed sample (Figure S3). These results from XRD, XPS, and SEM-EDS analyses indicate that the alloyed samples have been successfully obtained by modulating the Ag^+/Na^+ ratios in the precursor solution. In addition, inductively coupled plasma optical emission spectroscopy (ICP-OES) was performed to verify the actual Ag^+ concentration in the alloyed sample. The result indicates that the Ag^+/Na^+ ratios in the alloyed lattice almost match the original concentration of Ag^+ in the precursor solution (Table S1).

Lattice compression or expansion can alter the overlap of electronic wave function in perovskite systems in close proximity to their bandgap, thereby modifying their optical properties.^{23,24} To verify this, UV-vis absorption data for

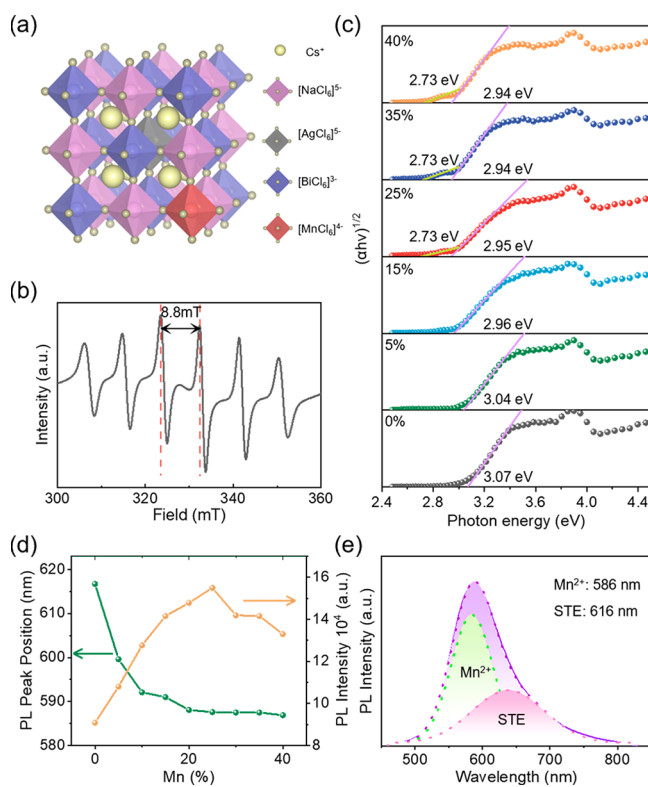


Figure 2. (a) Crystal structure of Mn^{2+} -doped $\text{Cs}_2\text{Na}_{1-x}\text{Ag}_x\text{BiCl}_6$. (b) Room-temperature EPR spectrum of Mn^{2+} -doped (25%) $\text{Cs}_2\text{Na}_{0.98}\text{Ag}_{0.02}\text{BiCl}_6$. (c) Tauc plots of Mn^{2+} -doped $\text{Cs}_2\text{Na}_{0.98}\text{Ag}_{0.02}\text{BiCl}_6$ samples with different Mn^{2+} (%) ratios in the precursor solution. (d) PL peak position and PL intensity vs Mn^{2+} doping ratio in the precursor solution. (e) Fitted PL spectra of the Mn^{2+} -doped (25%) $\text{Cs}_2\text{Na}_{0.98}\text{Ag}_{0.02}\text{BiCl}_6$. The fitted two peaks are 586 and 616 nm.

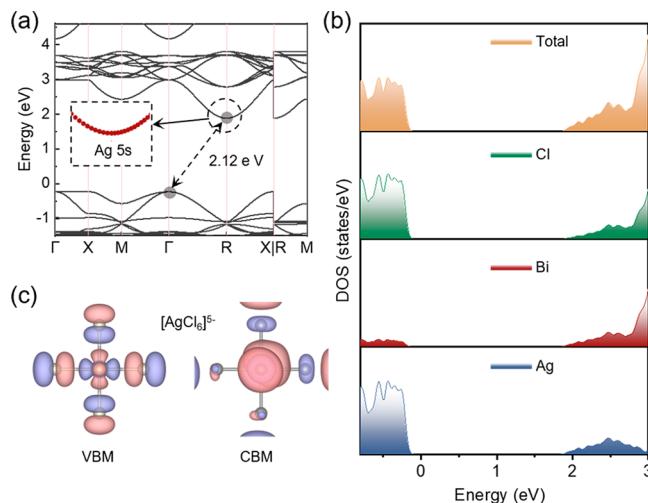


Figure 3. (a) Band structure of $\text{Cs}_2\text{Na}_{0.98}\text{Ag}_{0.02}\text{BiCl}_6$ computed using GGA-PBE functional. This 40-atom structural model was constructed by $2 \times 2 \times 2$ replication of the cubic unit cell ($Fm\bar{3}m$) of $\text{Cs}_2\text{NaBiCl}_6$. The enlarged view of band structure near the CBM is shown in the inset. (b) Total and partial density of states (DOS) plots of $\text{Cs}_2\text{Na}_{0.98}\text{Ag}_{0.02}\text{BiCl}_6$. (c) Wave functions of $\text{Cs}_2\text{Na}_{0.98}\text{Ag}_{0.02}\text{BiCl}_6$ on $[\text{AgCl}_6]^{5-}$ octahedra at the VBM and CBM and the corresponding isosurface are 7×10^{-8} and 5×10^{-8} e bohr⁻³, respectively.

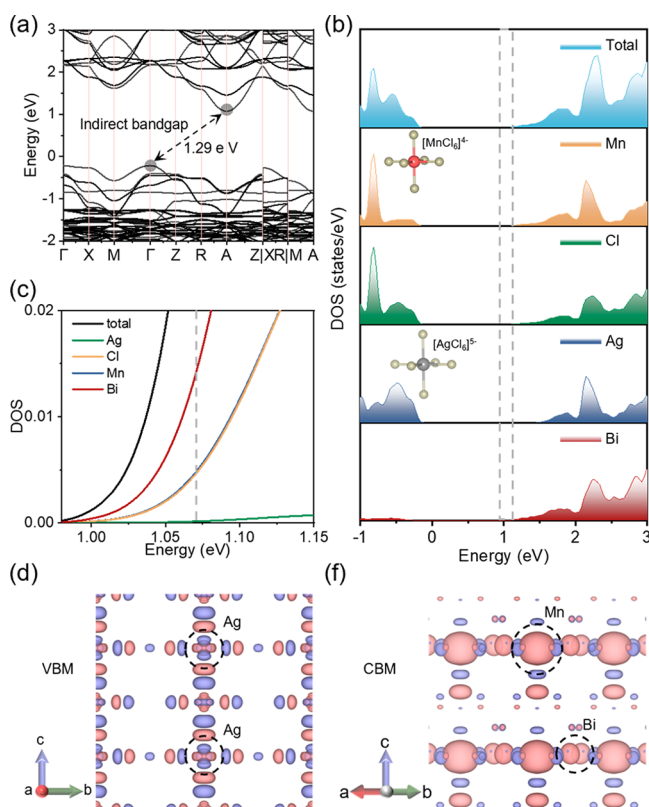


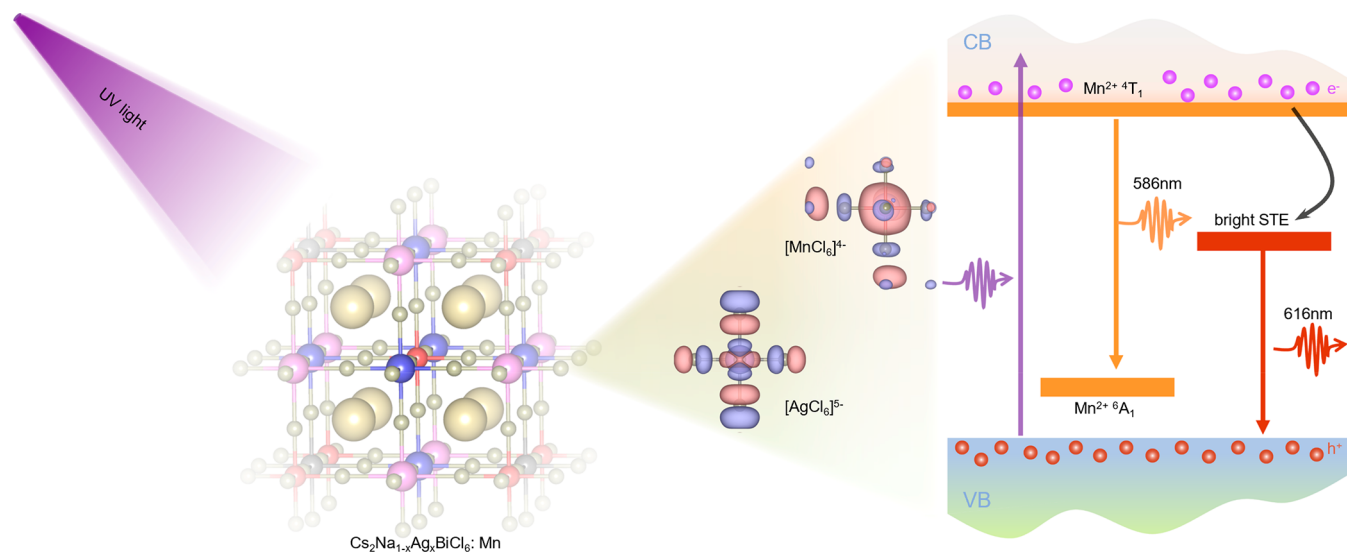
Figure 4. (a) Band structure of Mn^{2+} -doped (25%) $\text{Cs}_2\text{Na}_{0.98}\text{Ag}_{0.02}\text{BiCl}_6$ computed by spin-polarized DFT calculations using GGA-PBE functional. A Hubbard U parameter (DFT + U) value of 4.3 eV was introduced for Mn^{2+} to treat 3d correlations. This 40-atom structural model was constructed by a $2 \times 2 \times 2$ replication of the cubic unit cell ($Fm\bar{3}m$) of $\text{Cs}_2\text{NaBiCl}_6$. (b) Total and partial DOS plots of Mn^{2+} -doped (25%) $\text{Cs}_2\text{Na}_{0.98}\text{Ag}_{0.02}\text{BiCl}_6$. (c) Enlarged DOS plots of the area surrounded by gray dashed lines in (b). (d) Real-space wave functions of VBM and (f) CBM of Mn^{2+} -doped $\text{Cs}_2\text{Na}_{0.98}\text{Ag}_{0.02}\text{BiCl}_6$ (25%) with an isosurface of $5 \times 10^{-8} \text{ e bohr}^{-3}$.

samples of alloyed $\text{Cs}_2\text{Na}_{1-x}\text{Ag}_x\text{BiCl}_6$ were collected. Absorption spectra reveal that the bandgap of $\text{Cs}_2\text{Na}_{1-x}\text{Ag}_x\text{BiCl}_6$ can be tuned in the ultraviolet region by altering Ag^+/Na^+ ratios

(Figure 1b). As Ag^+ content increases in alloyed $\text{Cs}_2\text{Na}_{1-x}\text{Ag}_x\text{BiCl}_6$, the absorption band edge experiences a red-shift, as shown in the Tauc plot (Figure S4). The bandgap of alloyed sample gradually reduces from 3.36 to 2.98 eV when the concentration of Ag^+ rises from 0 to 5%. The dark STE state in the pure $\text{Cs}_2\text{NaBiCl}_6$ sample results in a very weak emission.^{20,25} Upon Ag^+ alloying, the $\text{Cs}_2\text{Na}_{1-x}\text{Ag}_x\text{BiCl}_6$ sample exhibits a broad orange-red PL emission peak at $\approx 616 \text{ nm}$ with a large Stokes shift. As the concentration of Ag^+ increases, the alloyed $\text{Cs}_2\text{Na}_{1-x}\text{Ag}_x\text{BiCl}_6$ sample experiences an evident increase in PL intensity with a maximum at $x = 2\%$ and then declines steadily thereafter (Figures 1c and S5). As with PL spectra, the PLQY of alloyed samples exhibit a similar trend with Ag^+ concentration, with a value is $42.06 \pm 1\%$ for the $\text{Cs}_2\text{Na}_{0.98}\text{Ag}_{0.02}\text{BiCl}_6$ sample (Figure S6). $\text{Cs}_2\text{Na}_{1-x}\text{Ag}_x\text{BiCl}_6$ alloys show notable shifts in absorption edges as the Ag^+/Na^+ ratio changes, but their PL peaks remain unchanged (Figure 1d). Combined with the previous research works, the broad emission band with large Stokes shift can be attributed to STE emission, which occurs in double perovskites with localized carriers and soft lattice.^{13,26,27} With Ag^+ concentrations varying from 2 to 10%, the effective PL lifetime of $\text{Cs}_2\text{Na}_{1-x}\text{Ag}_x\text{BiCl}_6$ alloys monotonically decreases from 4.83 to 1.10 μs (Figure S7). This indicates that the excess Ag^+ content would increase the nonradiative transition channels and ultimately accelerates PL dynamics.²³

To further enhance the PL efficiency, we doped the $\text{Cs}_2\text{Na}_{1-x}\text{Ag}_x\text{BiCl}_6$ system with Mn^{2+} ions. In general, Mn^{2+} dopants can introduce a new efficient emission channel from the ${}^4\text{T}_1 \rightarrow {}^6\text{A}_1$ transition.^{16,19} The XRD patterns of Mn^{2+} -doped $\text{Cs}_2\text{Na}_{1-x}\text{Ag}_x\text{BiCl}_6$ ($x = 0.02$) samples indicate that the samples retain the original cubic phase structure without any second phase impurity (Figure S8). XPS and SEM-EDS characterizations of the Mn^{2+} -doped (25%) $\text{Cs}_2\text{Na}_{0.98}\text{Ag}_{0.02}\text{BiCl}_6$ sample reveal that only a limited amount of Mn^{2+} dopants are contained in the crystal, despite a high feeding ratio of Mn^{2+} to Na^+ and Bi^{3+} (Figures S9 and S10), consistent with ICP-OES results. The concentration of Mn^{2+} increases from 0.09 to 2.63% in doped samples (Table S2), in sharp contrast to the initial ratios of $\text{Mn}^{2+}/(\text{Na}^+ + \text{Bi}^{3+})$ (5–35%) in the precursor solution. To explore the local coordination environment of Mn

Scheme 1. Illustration of the Emission Mechanism for Mn^{2+} -Doped $\text{Cs}_2\text{Na}_{0.98}\text{Ag}_{0.02}\text{BiCl}_6$ Sample



ions in the doped sample, electron paramagnetic resonance (EPR) spectroscopy was performed on the Mn^{2+} -doped $\text{Cs}_2\text{Na}_{0.98}\text{Ag}_{0.02}\text{BiCl}_6$ sample. The EPR spectrum exhibits a 6-fold splitting pattern with a hyperfine splitting constant of 8.8 mT (Figure 2b), suggesting that the doped Mn ions have the +2 oxidation state and are located in an octahedral coordination environment.^{14,22}

The bandgap of Mn^{2+} -doped $\text{Cs}_2\text{Na}_{0.98}\text{Ag}_{0.02}\text{BiCl}_6$ sample reduces from 3.07 to 2.94 eV with increasing Mn^{2+} concentration (Figures 2c and S11). This could be due to the size disparity among Mn^{2+} , Na^+ , and Bi^{3+} . Compared with undoped $\text{Cs}_2\text{Na}_{0.98}\text{Ag}_{0.02}\text{BiCl}_6$, Mn^{2+} doping results in an additional weak absorption peak at 430 nm. This may be contributed by the d–d transition of Mn^{2+} dopants, as it differs from the exciton absorption of the host.^{19,28} When Mn^{2+} ions are added to doped samples, the PL peak blue-shifts and remains unchanged at the high concentrations (Figure S12). The PL intensity of doped samples increases with the concentration of Mn^{2+} (0–25%). However, the PL intensity gradually decreases when the concentration exceeds 25% due to the quenching effect (Figure 2d).^{33,34} The highest PL intensity is obtained at 25% Mn^{2+} doping concentration, with a PLQY of $49.52 \pm 2\%$ (Figure S13). Interestingly, the PL spectrum of doped samples can be fitted into two peaks (Figure 2e): the STE emission (616 nm) of the host and a new emission peak at 586 nm. On the basis of the absorption result and previous work, it is possible that the new emission is characteristic emission of Mn^{2+} .^{15,29–31} Upon excitation at 430 nm, the doped samples show a narrow emission band around 583 nm (Figure S14). In addition, the new emission has a long lifetime of 0.28 ms, consistent with the spin-forbidden character of the ${}^4\text{T}_1\text{--}{}^6\text{A}_1$ transition of Mn^{2+} (Figure S15). Therefore, the new emission state at 586 nm in the doped system can be ascribed to ${}^4\text{T}_1\text{--}{}^6\text{A}_1$ transition of Mn^{2+} . The 3 nm red-shift might be caused by the coexistence of Mn^{2+} and STE emission states. Although Mn^{2+} and STE emission states coexist in the entire PL spectrum, the proportion of the Mn^{2+} emission has a positive correlation with the concentration of Mn^{2+} dopants, in contrast to the STE emission (Figure S16a). Excited electrons of the host may contribute to the efficient emission of Mn^{2+} by transferring directly to Mn^{2+} dopants.³² In addition, full width at half-maximum (FWHM) reduces from 106 to 73 nm after Mn^{2+} doping (Figure S16b).

Next, we explored the stability of all samples. The Mn^{2+} -doped sample maintains a high level of crystallinity and luminescence after three months of exposure to ambient light and atmosphere (Figure S17). The doped sample also shows high resistance to water when embedded in polydimethylsiloxane. Furthermore, the thermal stability of all samples was investigated by thermogravimetric analysis. Expectedly, the Mn^{2+} -doped sample exhibits an improved thermal stability; that is, the presence of Mn^{2+} increases the decomposition temperature relative to pure and alloyed samples (Figure S18). These findings confirm prior observations that Mn^{2+} dopants can enhance the stability of perovskites.^{14,35}

Density functional theory (DFT) calculations were performed to investigate electronic and optical effects of Ag^+ and Mn^{2+} dopants on $\text{Cs}_2\text{NaBiCl}_6$. For pure samples, the valence band maximum (VBM) and the conduction band maximum (CBM) are located at the k-points U/K and L , in good agreement with previous reports that bulk $\text{Cs}_2\text{NaBiCl}_6$ features an indirect bandgap (Figure S19a).^{36,37} It is evident from the total DOS plot that the VBM consists mainly

composed of 3p orbitals of Cl, whereas the CBM consists predominantly of 6p orbitals of Bi and 3p orbitals of Cl (Figure S19b). In addition, the wave functions of the pure sample are uniformly delocalized over the whole supercell (Figure S19c). There are some significant changes in the original electronic structure of the pure sample when the Na^+ at the center of the supercell is replaced by the Ag^+ ion. For instance, the alloyed sample has a smaller bandgap than the pure sample because the 5s orbitals of Ag^+ decrease the position of the CBM (Figure 3a),³⁸ which is qualitatively consistent with the experimental results. Additionally, the VBM of the alloyed sample is composed of Ag-4d and Cl-3p orbitals (Figure 3b). Ag^+ incorporation breaks the delocalized wave function of the pure sample and confines the wave function at $[\text{AgCl}_6]^{5-}$ octahedra by the surrounding $[\text{NaCl}_6]^{5-}$ barriers (Figure 3c). On the basis of previous reports, the $[\text{AgCl}_6]^{5-}$ octahedra with a strong Jahn–Teller distortion in the excited state plays a critical role in forming the bright STE state.^{13,20,25} Therefore, the weak photoluminescence efficiency can be attributed to the dark STE state in the pure $\text{Cs}_2\text{NaBiCl}_6$ sample, while the efficient orange-red emission originates from the bright STE state in the alloyed $\text{Cs}_2\text{Na}_{1-x}\text{Ag}_x\text{BiCl}_6$ samples. In addition, the $[\text{AgCl}_6]^{5-}$ octahedron has a smaller volume than $[\text{NaCl}_6]^{5-}$ (Figure S20), leading to a slight lattice distortion in alloyed samples. Therefore, alloyed samples exhibit a fast decay process at the early stage due to the nonradiative loss (Figure S7).

In the Mn^{2+} -doped structural model, one Na^+ ion and one Bi^{3+} ion are replaced by two Mn^{2+} ions. Upon Mn^{2+} doping, the bandgap further decreases (Figure 4a). A smaller Mn^{2+} ion would narrow the bandgap by promoting orbital overlap and enhancing electronic band dispersion due to the lattice constriction.^{21,39,40} VBM and CBM are located at the k-points Γ and A , indicating that doped samples keep the indirect bandgap character of the pure sample. Both the VBM and CBM belong to the same spin channels (spin-up) (Figure S21), which contributes to a highly efficient transition without the barrier from spin flip. The DOS plot shows that the VBM mainly originates from Ag-4d and Cl-3p orbitals and the CBM is composed with Bi-6p, Cl-3p, and slight Mn-3d orbitals (Figure 4b). Significantly, the enlarged DOS and band structure (Figures 4c and S22) exhibit pronounced orbital hybridizations among Mn-3d, Bi-6p, and Cl-3p at CBM. Moreover, the CBM wave function for the doped system is mostly localized on $[\text{BiCl}_6]^{3-}$ and $[\text{MnCl}_6]^{4-}$ octahedra (Figure 4f). These results confirm that the orbitals of Mn^{2+} participate in forming the conduction band edge in the doped system. Consequently, free electrons can transit directly from the excited state of the host to the Mn-3d orbitals and ultimately achieve efficient yellow-orange emission via the ${}^4\text{T}_1\text{--}{}^6\text{A}_1$ recombination of Mn^{2+} .

According to the above findings, a detailed mechanism for the highly efficient dual emission modes of Mn^{2+} -doped $\text{Cs}_2\text{Na}_{1-x}\text{Ag}_x\text{BiCl}_6$ is illustrated in Scheme 1. It has been reported that the generated free excitons relax to the ground state by nonradiative recombination due to the presence of the dark SET state in the pure sample.²⁰ Therefore, the pure sample exhibits weak photoluminescence efficiency. Interestingly, the dark SET state can be converted into a bright STE state by the introduced Ag^+ . Upon excitation, free excitons can transfer to the bright STE state in a rapid process,^{41–44} leading to a bright orange-red emission via radiative transition. In the Mn^{2+} -doped sample, there is a new emission channel except for

the bright STE state in the host. The 3d orbitals of the Mn^{2+} dopant can obtain excited electrons directly from the conduction band because they hybridize with the Bi-6p and Cl-3p orbitals at CBM, resulting in efficient yellow-orange emission from Mn^{2+} (586 nm). In this case, direct electron transfer not only avoids large energy losses caused by the energy difference between the host and Mn^{2+} but also shortens the time for energy transfer. Consequently, the efficient Mn^{2+} emission mode dominates the overall recombination progress, although the transfer process from the host to the STE state takes several picoseconds.^{25,45}

In summary, we have synthesized a series of Mn^{2+} -doped $\text{Cs}_2\text{Na}_{1-x}\text{Ag}_x\text{BiCl}_6$ samples with highly efficient dual emission modes. The alloyed $\text{Cs}_2\text{Na}_{1-x}\text{Ag}_x\text{BiCl}_6$ samples exhibit a bright orange-red STE emission with an intensity hundreds of times higher than that of the $\text{Cs}_2\text{NaBiCl}_6$ sample. Upon doping Mn^{2+} into the alloyed samples, an efficient orange-yellow emission of Mn^{2+} was observed, with a maximum PLQY of $49.25 \pm 2\%$ at 25% Mn^{2+} concentration. DFT calculations show that Ag^+ introduction is the critical factor for the formation of the bright STE state in $\text{Cs}_2\text{Na}_{1-x}\text{Ag}_x\text{BiCl}_6$ samples, which contributes to the bright orange-red emission around 616 nm. Moreover, the 3d orbitals of Mn^{2+} are involved in the CBM composition of the Mn^{2+} -doped sample, which enables direct electron transfer from the host to Mn^{2+} dopants and results in efficient Mn^{2+} emission around 586 nm. Our findings provide insight into the Mn^{2+} emission mechanism in Mn^{2+} -doped lead-free double perovskites as well as an effective method for optimizing the properties of lead-free double perovskites.

ASSOCIATED CONTENT

Supporting Information

The Supporting Information is available free of charge at <https://pubs.acs.org/doi/10.1021/acs.jpcllett.2c02694>.

Materials, synthesis method, characterizations, and corresponding calculation parameters (PDF)

AUTHOR INFORMATION

Corresponding Authors

Xiaogang Liu – Department of Chemistry, National University of Singapore, 117543, Singapore; orcid.org/0000-0003-2517-5790; Email: chmlx@nus.edu.sg

Guo Qin Xu – Department of Chemistry, National University of Singapore, 117543, Singapore; orcid.org/0000-0003-4671-7923; Email: chmxuqg@nus.edu.sg

Authors

Min Wang – Department of Chemistry, National University of Singapore, 117543, Singapore

Jing Lyu – Department of Chemistry, National University of Singapore, 117543, Singapore

Xian Qin – Department of Chemistry, National University of Singapore, 117543, Singapore

Shuo-Wang Yang – Institute of High Performance Computing, Agency for Science, Technology and Research, 138632, Singapore

Complete contact information is available at:

<https://pubs.acs.org/doi/10.1021/acs.jpcllett.2c02694>

Notes

The authors declare no competing financial interest.

ACKNOWLEDGMENTS

The authors acknowledge the support from the Academic Research Fund of the Ministry of Education, Singapore, and the National University of Singapore (A-0004533-00-00). Computational work was performed with high-performance computing facilities in NUS High Performance Computing (HPC) center, A*STAR Computational Resource Centre (ACRC), and National Supercomputing Centre (NSCC) in Singapore.

REFERENCES

- (1) Hui, W.; Chao, L.; Lu, H.; Xia, F.; Wei, Q.; Su, Z.; Niu, T.; Tao, L.; Du, B.; Li, D.; et al. Stabilizing Black-Phase Formamidinium Perovskite Formation at Room Temperature and High Humidity. *Science* **2021**, *371*, 1359–1364.
- (2) Kim, M.; Jeong, J.; Lu, H.; Lee, T. K.; Eickemeyer, F. T.; Liu, Y.; Choi, I. W.; Choi, S. J.; Jo, Y.; Kim, H.-B.; et al. Conformal Quantum Dot-SnO₂ Layers as Electron Transporters for Efficient Perovskite Solar Cells. *Science* **2022**, *375*, 302–306.
- (3) Ma, D.; Lin, K.; Dong, Y.; Choubisa, H.; Proppe, A. H.; Wu, D.; Wang, Y.-K.; Chen, B.; Li, P.; Fan, J. Z.; et al. Distribution Control Enables Efficient Reduced-Dimensional Perovskite LEDs. *Nature* **2021**, *599*, 594–598.
- (4) Pan, W.; Wu, H.; Luo, J.; Deng, Z.; Ge, C.; Chen, C.; Jiang, X.; Yin, W.-J.; Niu, G.; Zhu, L.; et al. Cs₂AgBiBr₆ Single-Crystal X-ray Detectors with A Low Detection Limit. *Nat. Photonics* **2017**, *11*, 726–732.
- (5) Fan, Q.; Biesold-McGee, G. V.; Ma, J.; Xu, Q.; Pan, S.; Peng, J.; Lin, Z. Lead-Free Halide Perovskite Nanocrystals: Crystal Structures, Synthesis, Stabilities, and Optical Properties. *Angew. Chem., Int. Ed.* **2020**, *59*, 1030–1046.
- (6) Swarnkar, A.; Ravi, V. K.; Nag, A. Beyond Colloidal Cesium Lead Halide Perovskite Nanocrystals: Analogous Metal Halides and Doping. *ACS Energy Lett.* **2017**, *2*, 1089–1098.
- (7) Tang, H.; Xu, Y.; Hu, X.; Hu, Q.; Chen, T.; Jiang, W.; Wang, L.; Jiang, W. Lead-Free Halide Double Perovskite Nanocrystals for Light-Emitting Applications: Strategies for Boosting Efficiency and Stability. *Adv. Sci.* **2021**, *8*, 2004118.
- (8) Greul, E.; Petrus, M. L.; Binek, A.; Docampo, P.; Bein, T. Highly stable, Phase Pure Cs₂AgBiBr₆ Double Perovskite Thin Films for Optoelectronic Applications. *J. Mater. Chem. A* **2017**, *5*, 19972–19981.
- (9) Slavney, A. H.; Hu, T.; Lindenberg, A. M.; Karunadasa, H. I. A Bismuth-Halide Double Perovskite with Long Carrier Recombination Lifetime for Photovoltaic Applications. *J. Am. Chem. Soc.* **2016**, *138*, 2138–2141.
- (10) Savory, C. N.; Walsh, A.; Scanlon, D. O. Can Pb-Free Halide Double Perovskites Support High-Efficiency Solar Cells? *ACS Energy Lett.* **2016**, *1*, 949–955.
- (11) Filip, M. R.; Hillman, S.; Haghighirad, A. A.; Snaith, H. J.; Giustino, F. Band Gaps of the Lead-Free Halide Double Perovskites Cs₂BiAgCl₆ and Cs₂BiAgBr₆ from Theory and Experiment. *J. Phys. Chem. Lett.* **2016**, *7*, 2579–2585.
- (12) Yang, B.; Chen, J.; Yang, S.; Hong, F.; Sun, L.; Han, P.; Pullerits, T.; Deng, W.; Han, K. Lead-Free Silver-Bismuth Halide Double Perovskite Nanocrystals. *Angew. Chem., Int. Ed.* **2018**, *57*, 5359–5363.
- (13) Luo, J.; Wang, X.; Li, S.; Liu, J.; Guo, Y.; Niu, G.; Yao, L.; Fu, Y.; Gao, L.; Dong, Q.; et al. Efficient and Stable Emission of Warm-White Light from Lead-Free Halide Double Perovskites. *Nature* **2018**, *563*, 541–545.
- (14) Locardi, F.; Cirignano, M.; Baranov, D.; Dang, Z.; Prato, M.; Drago, F.; Ferretti, M.; Pinchetti, V.; Fanciulli, M.; Brovelli, S.; et al. Colloidal Synthesis of Double Perovskite Cs₂AgInCl₆ and Mn-Doped Cs₂AgInCl₆ Nanocrystals. *J. Am. Chem. Soc.* **2018**, *140*, 12989–12995.

- (15) Das Adhikari, S.; Guria, A. K.; Pradhan, N. Insights of Doping and the Photoluminescence Properties of Mn-Doped Perovskite Nanocrystals. *J. Phys. Chem. Lett.* **2019**, *10*, 2250–2257.
- (16) Liu, W.; Lin, Q.; Li, H.; Wu, K.; Robel, I.; Pietryga, J. M.; Klimov, V. I. Mn²⁺-Doped Lead Halide Perovskite Nanocrystals with Dual-Color Emission Controlled by Halide Content. *J. Am. Chem. Soc.* **2016**, *138*, 14954–14961.
- (17) Su, X.; Lian, L.; Zhang, C.; Zhang, J.; Liu, S.; Zhu, S.; Gao, Y.; Luo, W.; Li, H.; Zhang, D. Enhanced Photoluminescence of Colloidal Lead-Free Double Perovskite Cs₂Ag_{1-x}Na_xInCl₆ Nanocrystals Doped with Manganese. *Adv. Opt. Mater.* **2021**, *9*, 2001866.
- (18) Wang, S.; Leng, J.; Sun, Q.; Zhao, C.; Jin, S. Efficient External Energy Transfer from Mn-Doped Perovskite Nanocrystals. *J. Phys. Chem. Lett.* **2021**, *12*, 1475–1480.
- (19) Su, B.; Molokeev, M. S.; Xia, Z. Unveiling Mn²⁺ Dopant States in Two-Dimensional Halide Perovskite toward Highly Efficient Photoluminescence. *J. Phys. Chem. Lett.* **2020**, *11*, 2510–2517.
- (20) Jiang, J.; Niu, G.; Sui, L.; Wang, X.; Zhang, Y.; Che, L.; Wu, G.; Yuan, K.; Yang, X. Transformation between the Dark and Bright Self-Trapped Excitons in Lead-Free Double-Perovskite Cs₂NaBiCl₆ under Pressure. *J. Phys. Chem. Lett.* **2021**, *12*, 7285–7292.
- (21) Zhang, L.; Liu, Z.; Sun, X.; Niu, G.; Jiang, J.; Fang, Y.; Duan, D.; Wang, K.; Sui, L.; Yuan, K.; et al. Retainable Bandgap Narrowing and Enhanced Photoluminescence in Mn-Doped and Undoped Cs₂NaBiCl₆ Double Perovskites by Pressure Engineering. *Adv. Opt. Mater.* **2022**, *10*, 2101892.
- (22) Majher, J. D.; Gray, M. B.; Strom, T. A.; Woodward, P. M. Cs₂NaBiCl₆:Mn²⁺—A New Orange-Red Halide Double Perovskite Phosphor. *Chem. Mater.* **2019**, *31*, 1738–1744.
- (23) Zhu, D.; Zito, J.; Pinchetti, V.; Dang, Z.; Olivati, A.; Pasquale, L.; Tang, A.; Zaffalon, M. L.; Meinardi, F.; Infante, I.; et al. Compositional Tuning of Carrier Dynamics in Cs₂Na_{1-x}Ag_xBiCl₆ Double-Perovskite Nanocrystals. *ACS Energy Lett.* **2020**, *5*, 1840–1847.
- (24) Zhou, J.; Rong, X.; Zhang, P.; Molokeev, M. S.; Wei, P.; Liu, Q.; Zhang, X.; Xia, Z. Manipulation of Bi³⁺/In³⁺ Transmutation and Mn²⁺-Doping Effect on the Structure and Optical Properties of Double Perovskite Cs₂NaBi_{1-x}In_xCl₆. *Adv. Opt. Mater.* **2019**, *7*, 1801435.
- (25) Han, P.; Mao, X.; Yang, S.; Zhang, F.; Yang, B.; Wei, D.; Deng, W.; Han, K. Lead-Free Sodium–Indium Double Perovskite Nanocrystals through Doping Silver Cations for Bright Yellow Emission. *Angew. Chem., Int. Ed.* **2019**, *58*, 17231–17235.
- (26) Yang, B.; Han, K. Ultrafast Dynamics of Self-Trapped Excitons in Lead-Free Perovskite Nanocrystals. *J. Phys. Chem. Lett.* **2021**, *12*, 8256–8262.
- (27) Smith, M. D.; Karunadasa, H. I. White-Light Emission from Layered Halide Perovskites. *Acc. Chem. Res.* **2018**, *51*, 619–627.
- (28) Vargas, B.; Reyes-Castillo, D. T.; Coutino-Gonzalez, E.; Sánchez-Aké, C.; Ramos, C.; Falcony, C.; Solis-Ibarra, D. Enhanced Luminescence and Mechanistic Studies on Layered Double-Perovskite Phosphors: Cs₄Cd_{1-x}Mn_xBi₂Cl₁₂. *Chem. Mater.* **2020**, *32*, 9307–9315.
- (29) Zhang, H.; Yao, J.; Yang, Y.; Fu, H. Tailoring Color-Tunable Dual Emissions of Mn²⁺-Alloyed Two-Dimensional Perovskite Quantum Wells. *Chem. Mater.* **2021**, *33*, 2847–2854.
- (30) Zheng, W.; Li, X.; Liu, N.; Yan, S.; Wang, X.; Zhang, X.; Liu, Y.; Liang, Y.; Zhang, Y.; Liu, H. Solution-Grown Chloride Perovskite Crystal of Red Afterglow. *Angew. Chem., Int. Ed.* **2021**, *60*, 24450–24455.
- (31) Ke, B.; Zeng, R.; Zhao, Z.; Wei, Q.; Xue, X.; Bai, K.; Cai, C.; Zhou, W.; Xia, Z.; Zou, B. Homo- and Heterovalent Doping-Mediated Self-Trapped Exciton Emission and Energy Transfer in Mn-Doped Cs₂Na_{1-x}Ag_xBiCl₆ Double Perovskites. *J. Phys. Chem. Lett.* **2020**, *11*, 340–348.
- (32) Zhou, G.; Jia, X.; Guo, S.; Molokeev, M.; Zhang, J.; Xia, Z. Role of Halogen Atoms on High-Efficiency Mn²⁺ Emission in Two-Dimensional Hybrid Perovskites. *J. Phys. Chem. Lett.* **2019**, *10*, 4706–4712.
- (33) Guria, A. K.; Dutta, S. K.; Adhikari, S. D.; Pradhan, N. Doping Mn²⁺ in Lead Halide Perovskite Nanocrystals: Successes and Challenges. *ACS Energy Lett.* **2017**, *2*, 1014–1021.
- (34) Nag, A.; Chakraborty, S.; Sarma, D. D. To Dope Mn²⁺ in a Semiconducting Nanocrystal. *J. Am. Chem. Soc.* **2008**, *130*, 10605–10611.
- (35) Sun, C.; Gao, Z.; Deng, Y.; Liu, H.; Wang, L.; Su, S.; Li, P.; Li, H.; Zhang, Z.; Bi, W. Orange to Red, Emission-Tunable Mn-Doped Two-Dimensional Perovskites with High Luminescence and Stability. *ACS Appl. Mater. Interfaces* **2019**, *11*, 34109–34116.
- (36) Yao, M.-M.; Wang, L.; Yao, J.-S.; Wang, K.-H.; Chen, C.; Zhu, B.-S.; Yang, J.-N.; Wang, J.-J.; Xu, W.-P.; Zhang, Q.; et al. Improving Lead-Free Double Perovskite Cs₂NaBiCl₆ Nanocrystal Optical Properties via Ion Doping. *Adv. Opt. Mater.* **2020**, *8*, 1901919.
- (37) Meng, W.; Wang, X.; Xiao, Z.; Wang, J.; Mitzi, D. B.; Yan, Y. Parity-Forbidden Transitions and Their Impact on the Optical Absorption Properties of Lead-Free Metal Halide Perovskites and Double Perovskites. *J. Phys. Chem. Lett.* **2017**, *8*, 2999–3007.
- (38) Locardi, F.; Sartori, E.; Buha, J.; Zito, J.; Prato, M.; Pinchetti, V.; Zaffalon, M. L.; Ferretti, M.; Brovelli, S.; Infante, I.; et al. Emissive Bi-Doped Double Perovskite Cs₂Ag_{1-x}Na_xInCl₆ Nanocrystals. *ACS Energy Lett.* **2019**, *4*, 1976–1982.
- (39) Ma, Z.; Li, Q.; Luo, J.; Li, S.; Sui, L.; Zhao, D.; Yuan, K.; Xiao, G.; Tang, J.; Quan, Z.; et al. Pressure-Driven Reverse Intersystem Crossing: New Path toward Bright Deep-Blue Emission of Lead-Free Halide Double Perovskites. *J. Am. Chem. Soc.* **2021**, *143*, 15176–15184.
- (40) Zhou, G.; Jiang, X.; Molokeev, M.; Lin, Z.; Zhao, J.; Wang, J.; Xia, Z. Optically Modulated Ultra-Broad-Band Warm White Emission in Mn²⁺-Doped (C₆H₁₈N₂O₂)PbBr₄ Hybrid Metal Halide Phosphor. *Chem. Mater.* **2019**, *31*, 5788–5795.
- (41) Li, S.; Luo, J.; Liu, J.; Tang, J. Self-Trapped Excitons in All-Inorganic Halide Perovskites: Fundamentals, Status, and Potential Applications. *J. Phys. Chem. Lett.* **2019**, *10*, 1999–2007.
- (42) Guo, Q.; Zhao, X.; Song, B.; Luo, J.; Tang, J. Light Emission of Self-Trapped Excitons in Inorganic Metal Halides for Optoelectronic Applications. *Adv. Mater.* **2022**, 2201008.
- (43) Zeng, R.; Zhang, L.; Xue, Y.; Ke, B.; Zhao, Z.; Huang, D.; Wei, Q.; Zhou, W.; Zou, B. Highly Efficient Blue Emission from Self-Trapped Excitons in Stable Sb³⁺-Doped Cs₂NaInCl₆ Double Perovskites. *J. Phys. Chem. Lett.* **2020**, *11*, 2053–2061.
- (44) Zeng, R.; Bai, K.; Wei, Q.; Chang, T.; Yan, J.; Ke, B.; Huang, J.; Wang, L.; Zhou, W.; Cao, S.; Zhao, J.; Zou, B. Boosting Triplet Self-Trapped Exciton Emission in Te(IV)-Doped Cs₂SnCl₆ Perovskite Variants. *Nano Res.* **2021**, *14*, 1551–1558.
- (45) Fei, L.; Yuan, X.; Hua, J.; Ikezawa, M.; Zeng, R.; Li, H.; Masumoto, Y.; Zhao, J. Enhanced Luminescence and Energy Transfer in Mn²⁺ Doped CsPbCl_{3-x}Br_x Perovskite Nanocrystals. *Nanoscale* **2018**, *10*, 19435–19442.